Three-Dimensional Structure of *meso*-Diaminopimelic Acid Dehydrogenase from *Corynebacterium glutamicum*[†,‡]

Giovanna Scapin,* Sreelatha G. Reddy, and John S. Blanchard

Department of Biochemistry, Albert Einstein College of Medicine, 1300 Morris Park Avenue, Bronx, New York 10461

Received July 5, 1996; Revised Manuscript Received August 15, 1996[⊗]

ABSTRACT: Diaminopimelate dehydrogenase catalyzes the NADPH-dependent reduction of ammonia and L-2-amino-6-ketopimelate to form *meso*-diaminopimelate, the direct precursor of L-lysine in the bacterial lysine biosynthetic pathway. Since mammals lack this metabolic pathway, inhibitors of enzymes in this pathway may be useful as antibiotics or herbicides. Diaminopimelate dehydrogenase catalyzes the only oxidative deamination of an amino acid of D configuration and must additionally distinguish between two chiral amino acid centers on the same symmetric substrate. The *Corynebacterium glutamicum* enzyme has been cloned, expressed in *Escherichia coli*, and purified to homogeneity using standard biochemical procedures [Reddy, S. G., Scapin, G., & Blanchard, J. S. (1996) *Proteins: Structure, Funct. Genet. 25*, 514−516]. The three-dimensional structure of the binary complex of diaminopimelate dehydrogenase with $NADP^+$ has been solved using multiple isomorphous replacement procedures and noncrystallographic symmetry averaging. The resulting model has been refined against 2.2 Å diffraction data to a conventional crystallographic *R*-factor of 17.0%. Diaminopimelate dehydrogenase is a homodimer of structurally not identical subunits. Each subunit is composed of three domains. The N-terminal domain contains a modified dinucleotide binding domain, or Rossman fold (six central β-strands in a 213456 topology surrounded by five α-helices). The second domain contains two α-helices and three β-strands. This domain is referred to as the dimerization domain, since it is involved in forming the monomer−monomer interface of the dimer. The third or C-terminal domain is composed of six β-strands and five α-helices. The relative position of the N- and C-terminal domain in the two monomers is different, defining an open and a closed conformation that may represent the enzyme's binding and active state, respectively. In both monomers the nucleotide is bound in an extended conformation across the C-terminal portion of the β-sheet of the Rossman fold, with its C4 facing the C-terminal domain. In the closed conformer two molecules of acetate have been refined in this region, and we postulate that they define the DAP binding site. The structure of diaminopimelate dehydrogenase shows interesting similarities to the structure of glutamate dehydrogenase [Baker, P. J., Britton, K. L., Rice, D. W., Rob, A., & Stillmann, T. J. (1992a) *J. Mol. Biol. 228*, 662−671] and leucine dehydrogenase [Baker, P. J., Turnbull, A. P., Sedelnikova, S. E., Stillman, T. J., & Rice, D. W. (1995) *Structure 3*, 693−705] and also resembles the structure of dihydrodipicolinate reductase [Scapin, G., Blanchard, J. S., & Sacchettini, J. C. (1995) *Biochemistry 34*, 3502−3512], the enzyme immediately preceding it in the diaminopimelic acid/lysine biosynthetic pathway.

meso-Diaminopimelate (*meso*-DAP),[1] a key intermediate in bacterial lysine biosynthesis and a constituent of cell walls of many eubacteria, can be formed by at least three different pathways: the succinylase pathway, in which succinylated intermediates are used (Kindler & Gilvarg, 1960; Berges et al., 1986), the acetylase pathway, in which acetylated intermediates are used (Sundharadas & Gilvarg, 1974), and the less common dehydrogenase pathway (White, 1986). Most bacteria appear to preferentialy utilize only one of the three pathways; thus *Escherichia coli* and Gram-positive bacteria use only the succinylase pathway, whereas exclusive use of the acetylase pathway is limited to certain *Bacillus* species (Sundharadas & Gilvarg, 1974). The dehydrogenase pathway has been found in *Bacillus sphaericus*, *Corynebacterium glutamicum*, and *Brevibacterium* sp. (Misono et al., 1986). Enzymes of the succinylase pathway have also been identified in *C. glutamicum* (Schrumpf et al., 1991). Since mammals lack the ability to synthesize diaminopimelate and require L-lysine in their diet, inhibitors of enzymes in these pathways may be effective, nontoxic antimicrobial agents or herbicides. Attempts to synthesize and test inhibitors for at least two of the enzymes in this pathway have been reported (Lam et al., 1988; Abbott et al., 1994).

In the dehydrogenase variant of the lysine biosynthetic pathway, the intermediate tetrahydrodipicolinate, common to all three pathways, is converted in a single step to the ultimate lysine precursor, *meso*-DAP, by a reaction catalyzed by *meso*-DAP dehydrogenase (DapDH, EC 1.4.1.16). The enzyme has been isolated, purified, and enzymatically characterized from *B. sphaericus*, *Brevibacterium* sp., and *C. glutamicum* (Misono & Soda, 1980; Misono et al., 1986b). It has been shown to be, in all three cases, a homodimer with a molecular weight of ca. 70 000 and is highly specific

[†] This work was supported by Grant AI33696 from the National Institutes of Health.

[‡] The atomic coordinates have been deposited with the Protein Data Bank, Brookhaven National Laboratory, PDB code 1DAP.

* Author to whom correspondence may be addressed.

[⊗] Abstract published in *Advance ACS Abstracts,* October 1, 1996.

[1] Abbreviations: DAP, diaminopimelate; DapDH, diaminopimelate dehydrogenase; $NADP^+$, β-nicotinamide adenine dinucleotide phosphate, oxidized form; RMS, root mean squared.

S0006-2960(96)01628-5 CCC: $12.00

Scheme 1: Reaction Catalyzed by Diaminopimelate Dehydrogenase

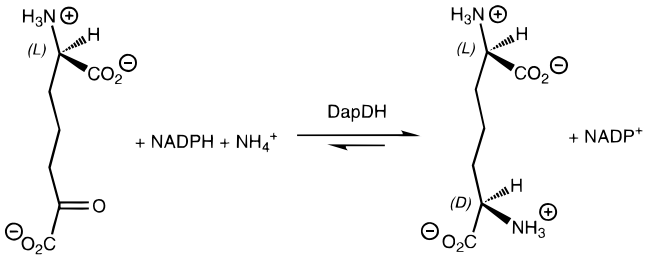

for *meso*-DAP and NADP(H) as substrates. All three enzymes have a similar pH optima for both the oxidative deamination and reductive amination reactions (10.5, 9.8, and 10.5, and 7.5, 7.6, and 8.5 for the *Bacillus*, *Corynebacterium*, and *Brevibacterium* enzymes, respectively; Misono & Soda, 1980; Misono et al., 1986a,b). The *Bacillus* enzyme is inactivated by bulky mercurials, suggesting the presence of a reactive cysteine near or at the active site. However, modification of the sulfhydryl group with small and uncharged groups did not affect the activity of the enzyme, suggesting that the sulfhydryl group does not play a role in catalysis (Misono et al., 1981). The *ddh* gene for the *C. glutamicum* enzyme has been sequenced (Ishino et al., 1986) and encodes a 320 amino acid polypeptide (molecular weight = 35 200) which has recently been overexpressed in *E. coli*, purified to homogeneity, and crystallized (Reddy et al., 1996). A BLAST sequence homology search (Alschul et al., 1990) demonstrated no significant homology with any protein in the Gene Bank but revealed a short stretch of amino acids in the N-terminal region similar to the dinucleotide binding fingerprint (Wierenga, 1986) of other dehydrogenases, including the glyceraldehyde-3-phosphate dehydrogenase of maize, *Saccharomyces cerevisiae*, *Sulfobulus solfataricus*, *E. coli*, and *Mesembryanthenum crystallinum*. For *C. glutamicum* DapDH this fingerprint region ends with two arginine residues, instead of an acidic residue, as expected for a NADP(H)-dependent enzyme.

DapDH catalyzes the unique, reversible $NADP^+$-dependent oxidative deamination of an amino acid of D configuration (Scheme 1). Recently, the three-dimensional structures of two L-amino acid dehydrogenases have been reported: glutamate dehydrogenase (GluDH; Baker et al., 1992a) and leucine dehydrogenase (LeuDH; Baker et al., 1995). While GluDH and LeuDH share about 20% sequence identity (Baker et al., 1995), and LeuDH is 50% identical to L-phenylalanine dehydrogenase (Britton et al., 1993), no significant homology has been found between DapDH and these other amino acid dehydrogenases. A similar result has been observed for dehydrogenases acting on L- and D-hydroxy acids; analysis of primary sequences showed that L- and D-hydroxy acid dehydrogenases form two distinct families (Grant, 1989) with little homology between the two families. On the other hand, comparisons of the three-dimensional structures of L-lactate dehydrogenase (LDH) and D-glycerate dehydrogenase (GDH; Goldberg et al., 1994) have identified a "striking geometric equivalence" of the protein elements in the active site of LDH and GDH, supporting a process of convergent evolution.

DAP dehydrogenase must distinguish between the two opposite amino acid chiral centers on the same symmetric molecule (Scheme 1). The enzyme is highly specific for *meso*-DAP, and for both the *Bacillus* and the *Corynebacterium* enzymes, L,L- and D,D-DAP are competitive inhibitors versus *meso*-DAP, with millimolar K_i values (Misono & Soda, 1980; Misono et al., 1986b). To probe the structural basis for this enzymatic stereospecificity, we initiated crystallographic studies of the *C. glutamicum* enzyme (Reddy et al., 1996). In this paper, we report the three-dimensional structure of the *C. glutamicum* DapDH·$NADP^+$ complex, solved and refined to a nominal resolution of 2.2 Å. The structure provides insights into the stereochemistry of proton transfer, substrate specificity, and enzyme mechanism and may offer the possibility of designing new inhibitors based on the active site structure.

EXPERIMENTAL PROCEDURES

Crystallization, Heavy Atom Derivative Preparation, and Data Collection. Recombinant *C. glutamicum* DapDH was expressed, purified, and crystallized in the presence of $NADP^+$ as previously described (Reddy et al., 1996). Two crystal forms were originally obtained, the first orthorhombic, space group $P2_12_12_1$, and the second monoclinic, space group $P2_1$. Only the monoclinic crystals were suitable for X-ray diffraction studies, and they were used for the three-dimensional structure determination of DapDH. These crystals have unit cell parameters of $a = 75.6$ Å, $b = 65.6$ Å, $c = 84.5$ Å, and $\beta = 106.5°$ and contain two molecules per asymmetric unit. A self-rotation function was calculated as described (Reddy et al., 1996), and the solution is a single peak with polar angles of $\phi = 30.0°$, $\psi = 90.0°$, and $\kappa = 180.0°$, indicating the presence of a single 2-fold noncrystallographic axis perpendicular to the *b* axis.

In order to use the multiple isomorphous replacement method to solve the structure of *C. glutamicum* DapDH, heavy atom soaks were performed on native crystals using a wide variety of heavy atom compounds. The heavy atom derivatives were prepared by soaking a native crystal in a 1 or 2 mM solution of the heavy atom in the crystallization buffer for 12−24 h. Reduction of the heavy atom concentration and/or the soaking time did not generate useful derivatives. X-ray diffraction data for native and all heavy atom-soaked crystals were collected on a Siemens multiwire area detector coupled to a Rigaku RU 200 rotating anode X-ray source, operating at 55 kV and 80 mA. Data were processed and reduced using the XENGEN software (Howard, 1986). Table 1 reports statistics on the data collected.

Structure Determination. Initial screening of heavy atom derivatives showed that not all soaked crystals were isomorphous with the native crystals, with variations in the unit cell parameters, especially the β angle, of approximately 3%. Examination of the data sets revealed that the extent of nonisomorphism was constant for various derivatives (see Table 1). One data set from a heavy atom-soaked crystal was then defined as a native data set, and difference Patterson maps were calculated with the suite PHASES (Furey & Swaminathan, 1990) and visually inspected. The bis-(ethylene diamino)platinum chloride (EDPC)-soaked crystal turned out to be not derivatized but, if used as native, gave strong signals in the difference Patterson maps calculated using K_2IrCl_6- and $Yb(NO_3)_3$-soaked crystals as *bona fide* derivatives. Patterson maps for both derivatives showed the presence of two major sites (plus a third minor one for the ytterbium derivative). The five heavy atom sites were

Table 1: Statistics for Native and Heavy Atom Derivative Crystals Used in the Three-Dimensional Structure Determination of *C. glutamicum* DapDH

data set	*a*, *b*, *c* (Å)	β (deg)	res (Å)	no. of observations[a]	no. of reflections[a]	% completeness[a]	$I/\sigma I$[a]	$R_{sym}(I)$[a]	R_{merge} on F[b]
native	75.9, 65.8, 84.5	106.6	2.2	135 992 (11329)	36 359 (4374)	89.2 (64.8)	7.7 (2.0)	7.8 (22.1)	
EDPC[c]	75.6, 66.6, 85.4	108.8	3.0	34 805 (4075)	15 067 (2200)	91.2 (80.3)	8.5 (2.2)	7.8 (18.4)	
K_2IrCl_6	76.8, 67.2, 85.4	109.1	3.0	31 910 (3843)	15 300 (2199)	91.7 (79.6)	8.5 (2.3)	7.2 (14.6)	9.9
$Yb(NO_3)_3$	76.6, 67.4, 85.4	109.4	3.0	29 964 (2844)	14 247 (1979)	85.5 (71.2)	6.0 (1.6)	10.4 (24.3)	7.9

[a] The numbers in parentheses represent measures in the last shell of resolution (2.3−2.2 Å for native data set and 3.1−3.0 Å for all others). [b] R_{merge} on F calculated using bis(ethylenediamino)platinum chloride (EDPC) as native. [c] This derivative was used as the native data set. See text for details.

Table 2: Statistics for Phase Calculation

derivative	*x*	*y*	*z*	occ	*B*	resolution (Å)	no. of reflections	phasing power	R_{Cullis}	R_{Kraut}
K_2IrCl_6						3.5	9415	1.69	0.578	0.112
IR1	0.012	−0.008	0.044	0.78	15.0					
IR2	0.456	0.244	0.478	0.84	15.0					
$Yb(NO_3)_3$						3.5	8896	1.52	0.629	0.089
YB1	0.299	−0.138	0.101	1.00	15.0					
YB2	0.441	0.392	0.231	1.32	15.0					
	0.349	0.355	0.391	0.49	15.0					

Average Figure of Merit versus Resolution (Å)

resolution	11.2	7.0	5.8	4.7	4.2	3.9	3.75	3.5	total
⟨FOM⟩	0.649	0.594	0.558	0.552	0.547	0.510	0.529	0.500	0.554

confirmed using the program VERIFY (S. L. Roderick, Albert Einstein College of Medicine). The program PHASIT was used to refine the position of the five sites and to calculate isomorphous MIR phases, using the EDPC data set as native. The resulting figure of merit for 8761 phased reflections to 3.5 Å with a 2σ cutoff on F was 0.56. Table 2 summarizes statistics for MIR phase calculation. Solvent flattening procedures (Wang, 1985) as implemented in DM (Cowtan, 1994) were used to improve the phases. The resulting map showed most of the secondary structural features, but several of the loops and connections were not observed. Reciprocal space averaging procedures, possible since there are two molecules per asymmetric unit, were then used to further improve the map. An initial mask was obtained by generating a solvent mask with DM and editing it using O (Jones et al., 1991) and MAMA (G. J. Kelywegt and T. A. Jones, to be published). The noncrystallographic symmetry (NCS) matrix was calculated from the heavy atom positions and the knowledge of the NCS axis.

Progress of the refinement was monitored using cross-validation methods (Roberts & Brunger, 1995; Cowtan & Main, 1996). Thirty cycles of electron density improvement using a combination of solvent flattening, noncrystallographic averaging, and histogram matching produced a map of much higher quality. This map allowed the tracing of about 75% of the polypeptide chain for one of the two molecules in the asymmetric unit. The second molecule was generated by applying the NCS matrix to the coordinates of the first molecule. In doing so it was evident that the NCS matrix did not apply to the entire asymmetric unit but only to the first 140 and the last 80 residues of the each polypeptide, since substantial differences between the two molecules are present in the middle region of the protein. Combined electron density maps [i.e., maps calculated combining MIR and model-based phases (Read, 1986)] were used to trace the polypeptide chain and to incorporate part of the amino acid sequence.

Structure Refinement. The protein coordinates (for 310 residues of one monomer and 313 residues of the other monomer, with approximately 75% of the side chains assigned) obtained from the combined electron density maps were used as a starting point for the refinement. During the early stages of the refinement, the simulated annealing procedure (slow cool) as implemented in the X-PLOR manual (Brünger et al., 1987; Brünger, 1992) was used, working with data between 8.0 and 3.0 Å (13 447 reflections with a 2σ cutoff applied, 88% of the possible data) and applying NCS restrains to residues 4−140 and 250−320. The conventional crystallographic *R*-factor went from 47.0% to 23.4% (*R*-free went from 48.5% to 39.3%), and the model maintained good geometry (RMS deviations for bond lengths and bond angles were 0.014 Å and 2.3°, respectively). Model-based phases were again combined with MIR phases, and the resulting electron density map was used to include all the remaining residues and side chains in both molecules in the model, with the exception of the first three residues, for which no electron density was visible.

The refinement was then continued against the original native data set. Forty cycles of rigid body refinement, followed by the simulated annealing, using data between 8 and 2.8 Å and applying NCS restraints to residues 4−140 and 241−320, were used to adjust the model to the new, slightly different unit cell parameters. The final *R*-factor for 18 524 reflections with a 2σ cutoff (97.4% of the possible) was 28.5% (*R*-free was 37.5%) with good geometry (RMS deviations for bond lengths and bond angles were 0.017 Å and 2.4°, respectively). Difference Fourier $((|F_o| - |F_c|)\phi_c)$ electron density maps allowed for the inclusion of all side chains but those of Asn111 (and Asn611 in the second molecule), Arg158, Gln191, Thr192, Arg208, Asn211 (and Asn711), Val221, Gln667, Glu673, and Lys766. The resolution was increased to 2.6 Å, and the *R*-factor after refinement was 25.8% (for 22 976 reflections with a 2σ cutoff, 96.1% of the possible data). Inspection of the resulting difference Fourier $((|F_o| - |F_c|)\phi_c)$ electron density map revealed the presence in both molecules of positive electron density that, based on the shape and location, could be attributed to the bound $NADP^+$. One nucleotide per molecule was modeled

Table 3: Statistics for the Refined Model of *C. glutamicum* DAP Dehydrogenase

reflections ($F > 2\sigma F$)	36150
resolution range (Å)	20.0−2.2
R-factor (%)	17.0
RMS bond lenghts (Å)	0.017
RMS bond angles (deg)	1.7
protein atoms	4926
ligand atoms	96
solvent atoms	183

⟨B⟩ (Å^2)	mol 1	mol 2
entire molecule	30.7	27.7
N-terminal region	26.7	25.2
C-terminal region	38.7	32.5
dimerization region[a]	23.7	22.7
ligand	27.7	22.7 (26.3, 29.2)[b]
solvent	43.7	37.3

[a] The dimerization region spans residues 122−145, 244−267, and 300−320 that are involved in the dimer formation. See text for complete description of the model. [b] Numbers in parentheses are the ⟨B⟩ for atoms of the two acetate molecules. See text for details.

into this electron density and included in the refinement. The final crystallographic *R*-factor for this model was 24.1% (*R*-free was 34.1%) for 22 976 reflections between 8.0 and 2.6 Å.

Least squares positional refinement, as implemented in TNT (Tronrud et al., 1988), was then included in the refinement strategy, using at first data between 20.0 and 2.4 Å (30 338 reflections with $F > 2\sigma$, 93% of the possible data). NCS were released during this stage of the refinement, and 120 water molecules were added to account for positive peaks of density in the difference Fourier ($(|F_o| - |F_c|)\phi_c$) electron density map that were greater or equal to three times the standard deviation of the map. The resulting *R*-factor was 20.2%, with RMS deviations for bond lengths and bond angles of 0.020 Å and 1.9°, respectively. Thirty additional cycles of TNT were then run, extending the resolution to 2.2 Å (36 150 reflections with $F > 2\sigma$, 86% of the possible data) including individual temperature factor refinement. During this last stage of refinement, inspection of the difference Fourier ($(|F_o| - |F_c|)\phi_c$) electron density map showed the presence of two acetate molecules near the nicotinamide portion of the bound cofactor in one of the two molecules. The two acetates were then included in the refinement, along with 53 additional water molecules. The final model has a crystallographic *R*-factor of 17.0%, with RMS deviations for bond lengths and bond angles of 0.017 Å and 1.7°, respectively. Table 3 summarizes statistics on the final model.

RESULTS AND DISCUSSION

Quality of the Structure. Figure 1 shows a ribbon diagram of the *C. glutamicum* DapDH three-dimensional structure. The current model of *C. glutamicum* DapDH contains 4926 protein atoms (two molecules per asymmetric unit), two molecules of NADP$^+$ (one per monomer), two molecules of acetate, and 183 solvent atoms. Each monomer contains 320 residues (numbered 1−320 and 501−820), and the side chains have been assigned for all residues except Met1, Met501, Thr502, Lys54, and Lys554 for which no electron density was visible in the final map. Table 3 reports statistics for the refined model. Figure 2 is a Ramachandran plot (as calculated with PROCHECK; Laskowski et al., 1993) of the

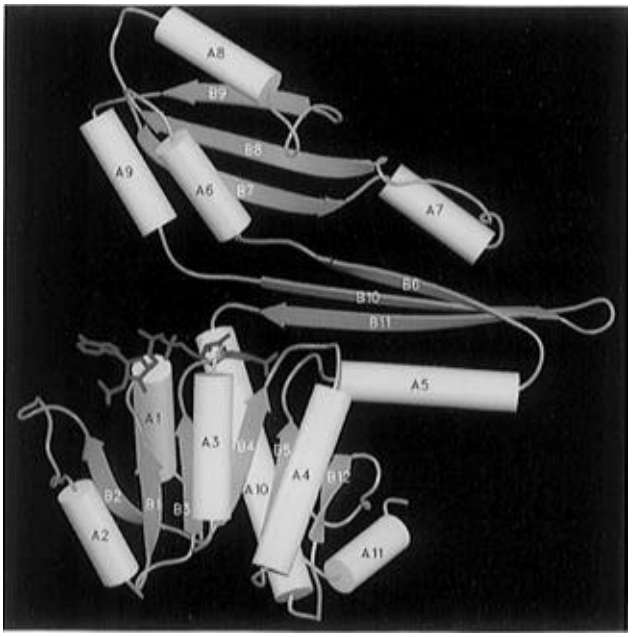

FIGURE 1: Ribbon diagram of the three-dimensional structure of one of the monomers of *C. glutamicum* DapDH. Helices A1 through A4 and A10 and β-strands B1 through B5 and B12 make up the dinucleotide binding domain. Helices A5 and A11 and β-strands B6, B10, and B11 compose the dimerization domain. Helices A6 through A9 and β-strands B7, B8, and B9 form the C-terminal domain. The bound NADP$^+$ is also displayed. This figure (and Figures 4a,b, 5a,b, and 7) was prepared with the program SETOR (Evans, 1993).

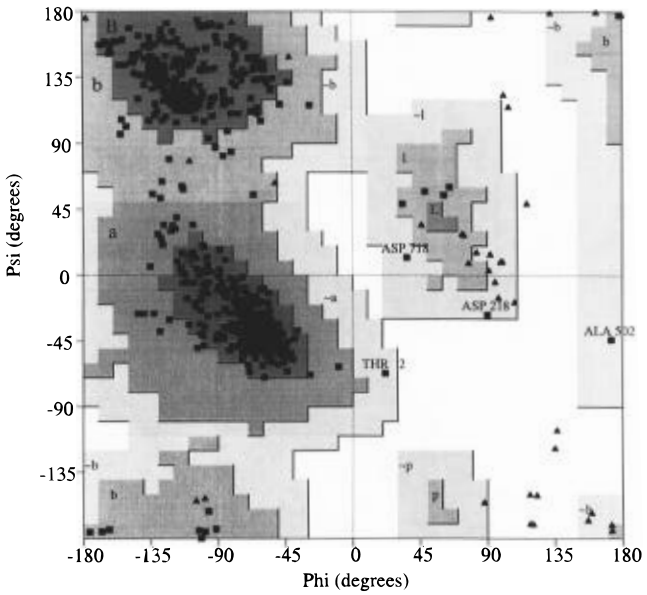

FIGURE 2: Ramachandran plot of the ϕ,ψ angles for the refined structure of *C. glutamicum* DapDH produced by the PROCHEK software (Laskowski et al., 1993). The most favored regions are shaded darkest (▲, glycines; ■, all other residues).

ϕ,ψ angles for the refined protein backbone. All residues fall within the allowed region of low conformational energy. Of the four residues located in the generously allowed regions, residues 2 and 502 belong to the N-terminal region of the protein that is flexible and exhibits weak electron density. Residues Asp218 (and Asp718) are located in a tight loop that connects A8 to B9, and the electron density for both side chains is well-defined.

Description of the Structure. *C. glutamicum* DapDH was reported to be a dimer in solution (Misono et al., 1986), and

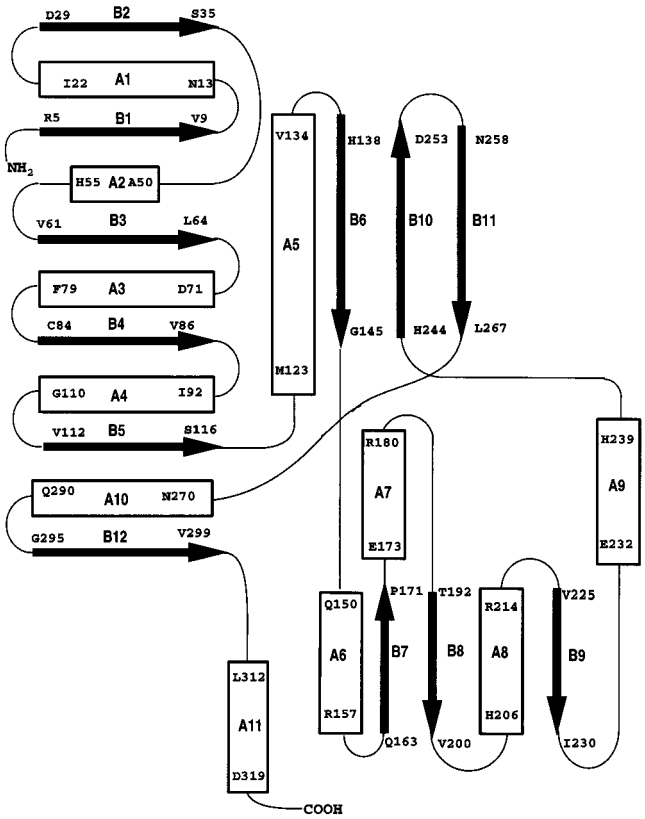

FIGURE 3: Schematic representation of the secondary structure elements in the three-dimensional structure of *C. glutamicum* DapDH.

the crystal form used to solve its three-dimensional structure contains one dimer per asymmetric unit. Figure 3 is a topology diagram of the secondary structure elements found in the monomer of *C. glutamicum* DapDH. The secondary structure elements that compose each monomer are identical for both subunits of the dimer, and for simplicity we will initially describe the structure of one monomer. The DapDH monomer can be divided into three domains. The first domain,which we will refer to as the dinucleotide binding domain, spans residues 1−118 and 269−299. It is composed of six β-strands (labeled in Figures 1 and 3 B1−B5 and B12) and five α-helices (A1−A4 and A10), arranged to form an α,β structure similar to that of the dinucleotide binding domain of many dehydrogenases [Rossmann et al., 1975; for a review see Brandën and Tooze (1992)]. The fold is not, however, that of a "classical" dinucleotide binding domain, with a symmetrical α,β structure built from two halves, each containing three β-strands connected by helices, with identical topology and similar structure. The observed DapDH fold is divided into two halves, but they are asymmetric: the first half contains two β-strands, B1 and B2, and one helix, A1, and it is connected to the second half by a long loop (residues 36−60) that also contains α-helix A2. The second half of the dinucleotide binding fold contains three β-strands B3, B4, and B5, and two α-helices, A3 and A4. Two more secondary structure elements are present in this second half of the dinucleotide binding domain, β-strand B12 and α-helix A10. These two secondary structural elements are from the C-terminal portion of *C. glutamicum* DapDH (Figure 3). A10 and A1 are parallel and located on the same side of the central six-stranded β-sheet; B12 is parallel and hydrogen bonded to B5.

The amino acid sequence "fingerprint" of the ADP binding $\beta\alpha\beta$ fold (Wierenga et al., 1986) spans residues Arg5−Arg37, that is, the B1−A1−B2 structural motif. The Gly-X-Gly-X-X-Gly consensus sequence is located at the carboxy-terminal end of β-strand B1 in the loop that connects it to α-helix A1. The $\beta\alpha\beta$ fold ends with a residue with a small side chain (Ser35), followed by two basic residues, Arg36 and Arg37, in the loop connecting B2 to A2, as expected for a NADP(H) binding protein (Baker et al., 1992a). DapDH shows an unusual fold for the dinucleotide binding domain, having two β-strands in the first half and three in the second half of the Rossmann fold, with topology $+1x$, $-2x$, $-1x$, $-1x$ (Richardson, 1981). This topology was first observed in flavodoxin (Watenpaugh et al., 1973; Burnett et al., 1974). Systems in which there are three β-strands in the first half and two β-strands in the second (with topology $+1x$, $+1x$, $-3x$, $-1x$) have been shown to exist in ferrodoxin−$NADP^+$ reductase (Karplus et al., 1991). NAD(P)H binding sites in which the topology of the strands of the central β-sheet is different, such as mixed parallel and antiparallel β-strands, have also been reported (Baker et al., 1992b; Davies et al., 1990). A 2 + 3 system is present in proteins that bind mononucleotides and have a modified Rossmann fold, as in the phosphoribosyltransferase family of enzymes (Scapin et al., 1994; Smith et al., 1994; Eads et al., 1995). Birktoft and Banaszak (1984) in an extensive review of the structure−function relationship among dinucleotide and FAD binding proteins stated that the identical topological folding unit for NAD binding was a subset of the six-stranded core domain originally proposed as the dinucleotide binding domain (Rao & Rossmann, 1973). This folding unit is composed of four parallel β-strands, with connectivity $+1$, $+1$, -3. Subsequent studies (Wierenga et al., 1985, 1986; Baker et al., 1992a) have suggested that the minimal conserved fold for the binding of the ADP moiety is the $\beta\alpha\beta$ unit formed by the first two β-strands of the dinucleotide binding domain and their connecting α-helix. DapDH represents an interesting variant in the common dinucleotide binding fold, since it contains only this minimal conserved fold for the ADP binding, with no additional secondary structural elements.

A four-residue loop between B5 and A5 (Figures 1 and 3) connects the dinucleotide binding domain to the second domain of *C. glutamicum* DapDH, which we will refer to as the "dimerization domain". This domain is composed of secondary structure elements that are not consecutive in the sequence: residues 122−145, 244−267 and 300−320. The dimerization domain contains two α-helices, A5 and A11, and three β-strands, B6, B10, and B11 (Figure 3). Met123−Val134 form A5, which is connected to B6 (His138−Gly145) by a sharp turn. Pro146−Ser149 lead into the third, C-terminal domain of DapDH, described below. The other two β-strands of the dimerization domain, B10 and B11, are connected by a diglycine type 1′ loop (Richardson, 1981). The three β-strands form an antiparallel β-sheet which is partially shielded from solvent by A5. The third portion of the dimerization domain, residues 300−320, contains a long loop that departs from the N-terminal domain and ends with α-helix A11 (Leu312−Asp319).

Residues 150−239 compose the C-terminal domain of *C. glutamicum* DapDH; this third domain contains four helices, A6, A7, A8, and A9, and three β-strands, B7, B8, and B9. α-Helices A6 and A8 are antiparallel to one another and

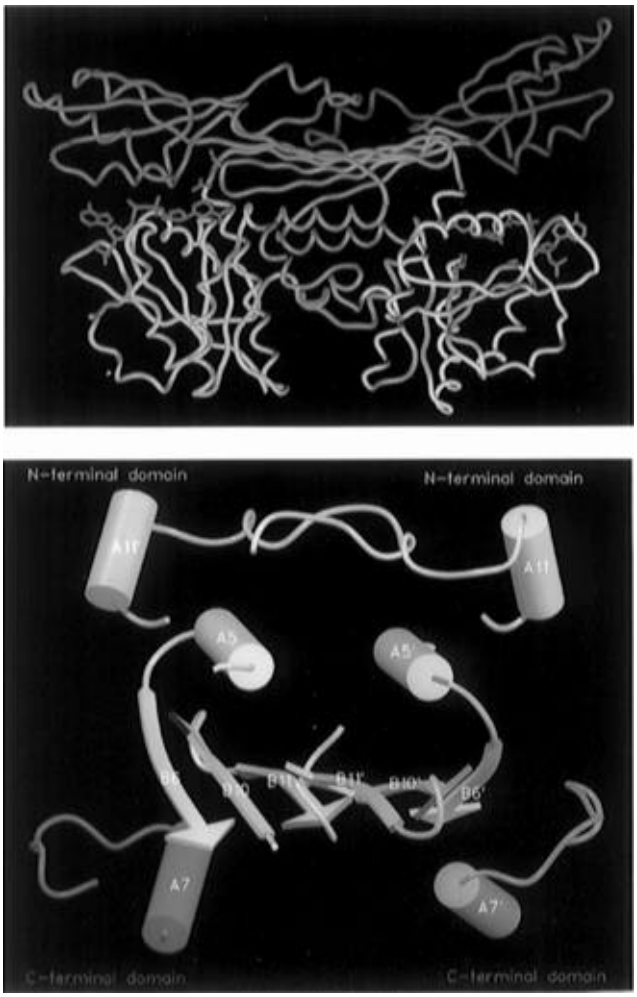

FIGURE 4: Ribbon diagram of the DapDH dimer. (a, top) Full view of the dimer. The three domains in the monomers are represented with different colors for monomer 1 and 2: yellow and light blue for the N-terminal domains; orange and blue for the dimerization domains; and red and dark blue for the C-terminal domains. The bound $NADP^+$ is shown in green. (b, bottom) Close-up of the dimerization domain (residues 122−145, 244−267, and 300−320) that shows the three layers into which the domain can be divided (see text for a complete discussion). A7 and A7′ belong to the C-terminal domain but, as described in the text, are interacting with residues of the dimerization domain.

together with β-strands B7, B8, and B9 form a mixed $\alpha\beta$ sandwich (Richardson, 1981). α-Helix A7 and the following 11-residue loop extend toward and partially cover the middle region of the dimerization domain β-sheet. α-Helix A9 is located on the opposite side of the $\alpha\beta$ sandwich from A6 and A8 and leads to strand B10 of the dimerization domain through residues Thr240−Pro243.

C. glutamicum DapDH Quaternary Structure. C. glutamicum DapDH has been reported to be a dimer in solution (Misono et al., 1986), and the protein crystallized with a dimer in the asymmetric unit. The two monomers are related by a limited noncrystallographic 2-fold axis, and the interface between the two subunits is quite extensive. The molecular surface for each monomer, as calculated with GRASP (Nicholls et al., 1991), is approximately 12 900 Å^2, and the formation of the dimer buries about 1900 Å^2 (15% of the surface) per monomer. Figure 4a is a ribbon diagram of the dimer. Interactions between the two monomers are made between residues of the two dimerization domains, with additional interactions between α-helix A11 and the N-terminal domain (Figure 4b). The β-sheets of the two dimerization domains are paired in an antiparallel way and form a six-stranded antiparallel β-sheet (B6−B10−B11−B11′−B10′−B6′). This mode of dimerization has been reported in other structures, including DHPR (Scapin et al., 1995), GluDH (Baker et al., 1992b), and LeuDH (Baker et al., 1995). The side of the β-sheet facing the N-terminal domain in Figure 4b is completely shielded from solvent by α-helices A5 and its antiparallel symmetry mate A5′. Both A5 and A5′ also interact with residues 300−320 of the other monomer: this C-terminal tail departs from one monomer and moves into the other monomer, so that the loop crosses perpendicularly A5 and A5′. The axes of A5 and A5′ are about 10 Å apart and 10 Å away from the backbone of the β-sheet, and the region between them is completely filled with hydrophobic and aromatic side chains that make up a hydrophobic core. The other side of the β-sheet is partially covered by A7 and the loop that connects it to B8 and their symmetry mates. This leaves the two central β-strands (B11 and B11′) exposed to the solvent, and analysis of the amino acid sequence shows that they contain alternating hydrophobic and hydrophilic residues, with the hydrophobic side chain facing the hydrophobic core of the dimer and the hydrophilic side chains facing, and interacting with, the solvent.

The two monomers that make up the *C. glutamicum* DapDH dimer are not identical. Overlaying the two molecules by applying the noncrystallographic symmetry matrix shows that, while an almost perfect match exists for residues of the dinucleotide binding and dimerization domains (the RMS for the Cα position is 0.370 Å and for all atoms is 1.02 Å, as calculated with X-PLOR), a large difference exists between residues of the two C-terminal domains (Figure 5). Overlaying the two monomers using either the N-terminal and dimerization domains or the C-terminal domain (Figure 5, panels a and b, respectively) shows that there is a rigid body movement of the two domains, which can be described as a 25° rotation of one region with respect to the other around an ideal axis that connects two interregion linkages (Gly145−Gly147 and H239−G241). These two hinges move through two large torsional angle changes: $\Delta\psi$(Gly145) = 28°, and $\Delta\psi$(Thr240) = −30°. The two monomers in the dimer exist in either an "open" or a "closed" conformation. In the open monomer, the C-terminal portion of the nucleotide binding domain is exposed to the solvent, while in the closed monomer this C-terminal portion is covered by atoms of the C-terminal domain, specifically α-helices A6 and A9. The RMS deviation for Cα atoms of the two C-terminal domains is 1.18 Å, significantly higher than the corresponding value for the N-terminal domains. The only significant differences in the C-terminal domains are observed for α-helix A7 and the following loop (Figure 5b). Although A7 and the loop are part of the C-terminal domain they interact with atoms of the dimerization domain, and thus are not subject to the same noncrystallographic symmetry as the C-terminal domain.

Dinucleotide Binding Site. Crystals of *C. glutamicum* DapDH used in the three-dimensional structure determination were obtained in the presence of $NADP^+$. Analysis of $((|F_o| - |F_c|)\phi_c)$ difference Fourier electron density maps showed the presence of continuous positive electron density across the C-terminal portion of the β-sheet of the N-terminal domain in both monomers. On the basis of its location and

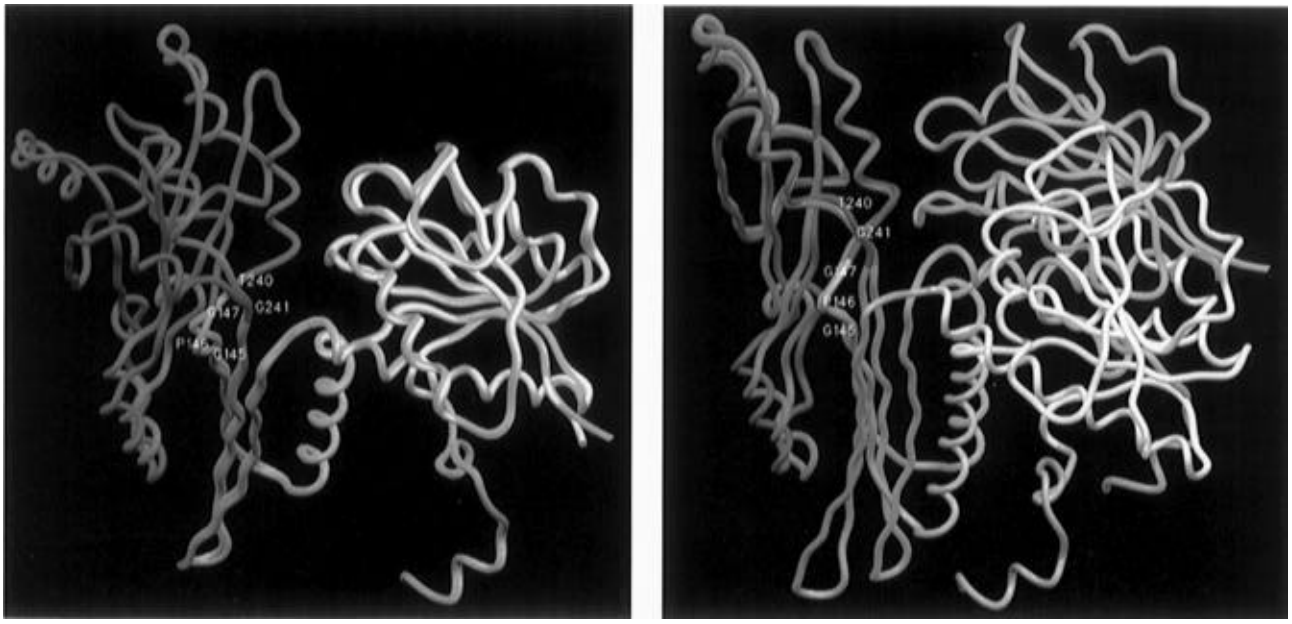

FIGURE 5: Overlay of the Cα trace of the two monomers in the DapDH dimer: (a, left) overlay of the dinucleotide binding and dimerization regions; (b, right) overlay of the C-terminal region.

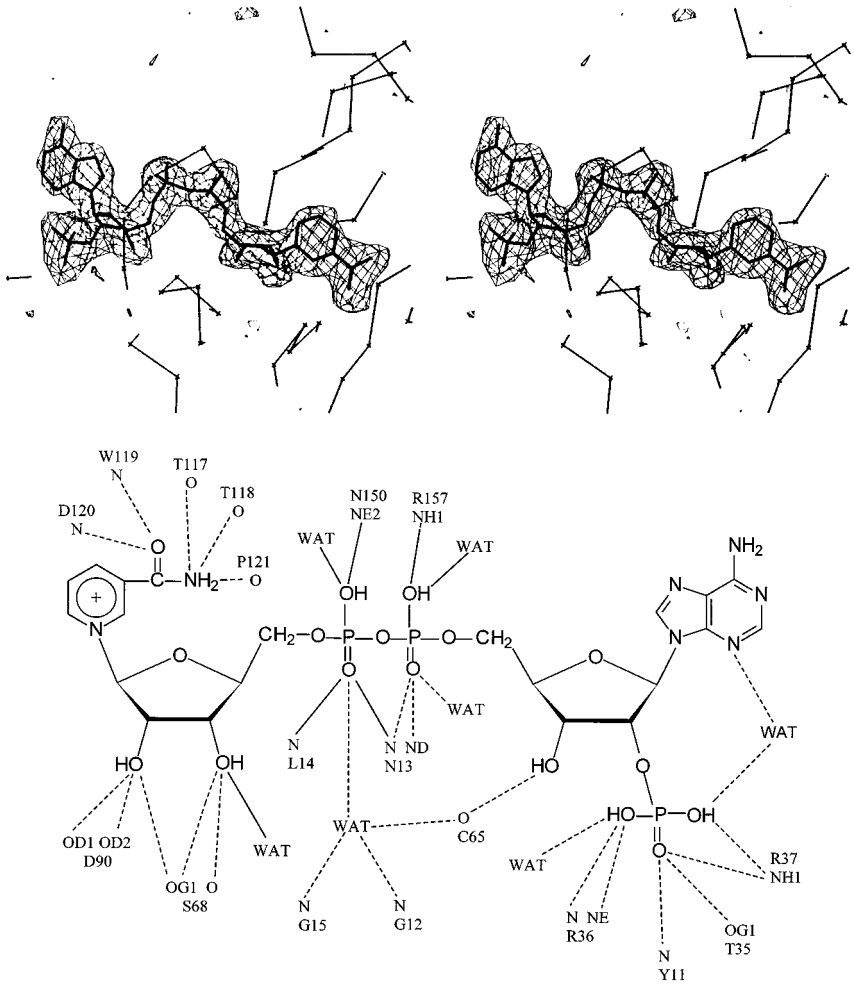

FIGURE 6: (a, top) Stereo diagram of the difference Fourier electron density map for the DapDH·$NADP^+$ complex used to locate the bound cofactor. The map was calculated to 2.7 Å. (b, bottom) Schematic diagram of the interactions made by the bound $NADP^+$ with protein atoms. Dotted lines represent interactions present in both molecules and continuous lines interactions present only in the closed monomer.

its shape, this electron density was fitted as bound $NADP^+$. Figure 6a is a stereoview of the $NADP^+$ electron density, and Figure 6b is a schematic representation of the interactions made by the bound cofactor with protein atoms in both molecules. The nucleotide is bound in an extended conformation in a similar manner in both monomers (the RMS deviation for atoms of the two $NADP^+$ molecules is 0.25 Å). The small differences in the interactions with protein

atoms are due to the different conformations of the two monomers rather than the nucleotide, and we will describe the interactions that occur between $NADP^+$ and protein atoms in one monomer, pointing out only the differences in the other monomer.

(A) Adenine and Adenine Ribose. The adenine is located in a very solvent-exposed area, in a *syn* configuration. The adenine ring is within van der Waals distance from the side chain of Arg37 and makes a single hydrogen bond between N3 and an ordered water molecule. This lack of specific interaction between base and protein atoms would suggest that the enzyme would be able to use base analogs such as nicotinamide hypoxanthine dinucleotide 2′-phosphate (NHD-PH) as cofactors. The adenosyl ribose has a 2′-exo, 3′-endo pucker, and the O3′ hydroxyl makes a single hydrogen bond to the main chain oxygen of Cys65. The 2′-phosphate sits in a pocket bordered by the side chain atoms of Thr35, Arg36, and Arg37 and the main chain atoms of Gly10 and Phe11. It makes eight hydrogen bond interactions (Figure 6b) with surrounding atoms, two of which are ordered water molecules. The large number of hydrogen bonds to the 2′-phosphate explains the high specificity of *C. glutamicum* DapDH for NADP(H) (Misono et al., 1986), as has been observed in other NADPH-specific dehydrogenases and reductases (Karplus & Schulz, 1989; Bystroff et al., 1990; Karplus et al., 1991).

(B) Pyrophosphate. The pyrophosphate moiety is located directly over the "dinucleotide binding helix" (Hol et al., 1978; A1) and interacts with main chain and side chain atoms of residues of the loop that connects β-strand B1 to α-helix A1. In the open monomer, the bottom portion of the pyrophosphate (as seen in Figure 3) faces the protein and forms four hydrogen bonds, two with protein atoms and two with ordered water molecules. One of these water molecules is part of an extensive hydrogen bond network that involves three additional protein atoms and can thus be considered as a "structural" water, important in the nucleotide binding. The upper portions of the pyrophosphate and the nicotinamide moiety are exposed to the bulk solvent and do not form any specific interaction with protein or solvent atoms. In contrast, in the closed monomer, the pyrophosphate and nicotinamide moieties are completely covered with protein atoms, which form a narrow channel of about 6 Å in diameter and 17 Å in length. The pyrophosphate forms six additional hydrogen bonds in the closed monomer, four with residues from the N-terminal and C-terminal domains of DapDH and two with water molecules. The much more extensive network of hydrogen bonds to $NADP^+$ observed in the closed monomer is reflected in the lower temperature factors found for atoms of the nucleotide (Table 3).

(C) Nicotinamide and Nicotinamide Ribose. The nicotinamide ribose is located deep inside the cradle and forms, in both monomers, five hydrogen bonds with protein atoms (Figure 6b). In the closed monomer, the ribose 3′-hydroxyl additionally interacts with an ordered solvent molecule. The nicotinamide carboxamido group forms, in both monomers, five hydrogen bonds with protein atoms (Figure 6b), and the nicotinamide ring is rigidly bound within a pocket formed by protein atoms (Branden & Tooze, 1991). In this conformation, the C4S hydrogen points toward the dinucleotide binding domain, while the C4R faces the C-terminal domain, where we postulate the substrate binding site is located. On this basis, DapDH can be classified as a type A reductase (transfer of the *pro-R* hydrogen). This is different from all the other known amino acid dehydrogenases, for which the transfer involves the *pro-S* hydrogen (Brunhuber & Blanchard, 1994). The stereospecificity determined by these structural studies is in contrast with the reported *pro-S* stereospecificity for the *B. sphaericus* DapDH (Misono & Soda, 1980).

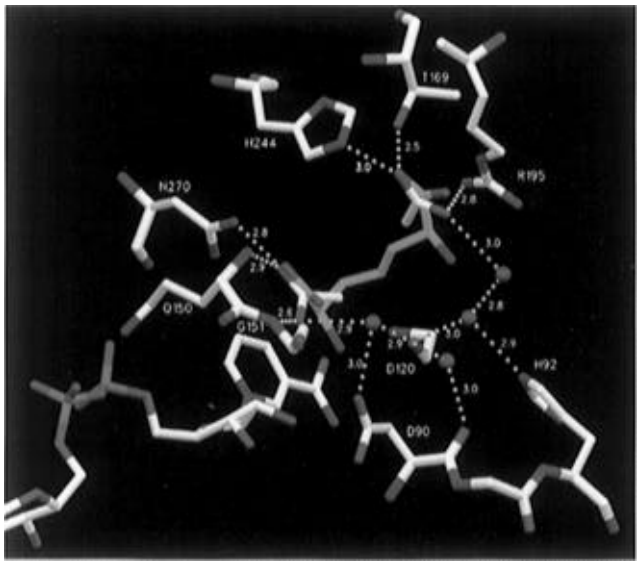

FIGURE 7: Close-up of the binding site of the acetate molecules in DapDH. A molecule of DAP (carbon atoms are in blue) has been overlaid onto the two acetates.

Substrate Binding Site. Although the DapDH crystals used in these studies were obtained in the presence of $NADP^+$, and in the absence of added DAP, analysis of the binary complex may reveal features that allow for the suggestion of a substrate binding site. The C4 position of $NADP^+$ is near the C-terminal domain; during the last cycle of refinement, analysis of the $(|F_o| - |F_c|)\phi_c$ difference Fourier electron density map in this area revealed, in the closed monomer, v-shaped peaks of positive electron density greater than 3σ that could not be modeled as ordered water molecules. Crystals of the DapDH·$NADP^+$ complex were grown in the presence of magnesium acetate (Reddy et al., 1996). These positive density peaks were located in a region rich in positively charged residues, making the assignment of the density to a bound metal ion, i.e., Mg^{2+}, unlikely. Alternatively, acetate molecules seemed good candidates, from both the location and the shape of the electron density. Two acetate molecules were modeled inside this electron density and refined to average temperature factors of 26.3 and 29.2 $Å^2$. Four ordered water molecules were found near the two acetate molecules in the closed monomer. In the open form of the protein, no similar v-shaped electron density was observed. Figure 7 is a view of the two acetate molecules' binding site. The acetate binding site is a roughly round cavity, bordered by main chain and side chain atoms of residues that belong to all three protein domains: Asp90−His92 and Leu265−Pro271 belong to the dinucleotide binding domain, Gly118−Met122, Thr142−Ser149 and His244 are part of the dimerization domain, and Gln150−Gly151, Thr169, and Arg195 belong to the C-terminal domain. Of the two acetate molecules, the one closer to the $NADP^+$ nicotinamide ring (Figure 7) forms three hydrogen bonds with the main chain nitrogen of Gln150 and Gly151 and the side chain nitrogen of Asn270 (2.6, 2.9, and 2.8 Å,

respectively). It also interacts with an ordered solvent molecule (2.9 Å), which is part of a network of hydrogen bonds involving a second water and the main chain nitrogen and side chain oxygen of Asp90 (Figure 7). The second acetate molecule hydrogen bonds to the side chain nitrogen of His244 (3.0 Å), the side chain oxygen of Thr169 (2.5 Å), the side chain nitrogen of Arg 195 (2.8 Å), and a third ordered water molecule found in the binding site (3.0 Å). This water is hydrogen bound to the fourth binding site water molecule, which is interacting with the side chain nitrogen of His92 and the main chain oxygen of Asp120 (see Figure 7). Of the four water molecules described above, the second and the fourth are observed in the open monomer, where they occupy similar positions and interact with the same protein atoms. In addition to these specific interactions with the bound acetate molecules, the closed form of the monomer shows two more hydrogen bond interactions with the pyrophosphate moiety (described above) and new protein−protein interactions (the side chain of Asp218 with the side chain of Asn51 and the side chain of Tyr219 with the side chain of Asp90). In the open form of the monomer, all the atoms involved in the previously described hydrogen bond interactions with substrate or protein atoms either are facing the bulk solvent (Asn91, Asp218, Tyr219, His244), are hydrogen bonding to water molecules that line the open cleft (Asp90, Asn270, Arg195), or are loosely interacting (the average distance is 3.3 Å) with adjacent side chains (Thr169 with Gln167 and Gln150 with Arg157 and Asp154).

The distance between the two acetate carboxylates is about 5 Å. The DapDH substrate, DAP, has two carboxylates separated by about 5 Å if the five intervening carbon atoms are in an all-trans conformation. We attempted to model a molecule of DAP into the two acetate binding sites, and the fit is good (Figure 7, carbon atoms are in blue). In this model, the α-carbon of the D center of DAP is 2.8 Å away from the nicotinamide C4, a reasonable distance for hydride transfer to occur. As discussed above, in the open monomer, both the nicotinamide portion of $NADP^+$ and the substrate binding site are exposed to the bulk solvent, while in the closed monomer they are surrounded by protein atoms and are solvent inaccessible, with the exception of discrete water molecules in the catalytic site. It is reasonable to propose that the open protein conformation represents the "binding" form of the enzyme, while the closed protein conformation represents the "active" form of the enzyme, as has been proposed for other dehydrogenases (i.e., GluDH; Stillman et al., 1993). Binding of NADP(H) alone does not cause the protein to close into the active form (the second monomer in the dimer has $NADP^+$ bound and is in a open conformation); the rigid body movement of the two domains may occur only after binding of substrate or substrate analogs. The kinetic mechanism has been proposed to be ordered sequential (Misono & Soda, 1980), with $NADP^+$ binding first, followed by DAP, and ammonia, ketopimelate, and NADPH being released in that order, and these structural studies support the kinetic mechanism data.

The structure determined here, showing one monomer of the dimer in an open conformation and the second in a closed, substrate-bound conformation, may be due either to crystal lattice contact stabilization of this dimer or to an intrinsic "half-of-the-sites" reactivity exhibited by DapDH. Kinetic studies to distinguish between these possibilities are underway. We are also presently attempting to prepare crystals with D,L-DAP bound at the active site to explore additional details about substrate binding, in particular, the enzymatic discrimination between the L and D stereo centers of DAP.

Structural and Functional Relationship to Other Amino Acid Dehydrogenases. DAP dehydrogenase is an amino acid dehydrogenase that acts on a chiral center with D configuration. All other 16 known NAD(P)H-dependent amino acid dehydrogenases act on L centers (Brunhuber & Blanchard, 1994). Recently, the three-dimensional structures for the *Clostridium symbiosium* GluDH (Baker et al., 1992a), *B. sphearicus* LeuDH (Baker et al., 1995), and *Pyrococcus furiosus* GluDH (Yip et al., 1995) have been reported. The folds of LeuDH and GluDH are very similar (Baker et al., 1995), and both are formed by two domains separated by a deep cleft; the N-terminal domain is the substrate binding domain and is responsible for subunit assembly, while the C-terminal domain contains the dinucleotide binding fold (Baker et al., 1992a, 1995). Although the quaternary structure for the two dehydrogenases is different, GluDH being an hexamer with 32 symmetry and LeuDH an octamer with 42 symmetry, the dimers that make up both hexamer and octamer are fairly similar. The differences in quaternary structure have been proposed to be part of the substrate recognition (Baker et al., 1995). A qualitative comparison between the Cα trace of GluDH, LeuDH, and DapDH is shown in Figure 8. The overall structures are remarkably similar; they all contain two domains (in the case of DapDH, one is subdivided into what we defined as dimerization and C-terminal domains) separated by a deep cleft. One of the domains is a dinucleotide binding domain and the other is defined as a substrate binding domain, and in all three dehydrogenases this second domain contains a mixed, twisted six-stranded β-sheet surrounded by α-helices.

Britton et al. (1993) have suggested, on the basis of the primary sequence alignments of GluDh, PheDH, and LeuDH and the crystalline structure of GluDH, that there may be a "core" structure common to amino acid dehydrogenases, composed of the six β-strands and three α-helices of the substrate binding domain, five β-strands and four α-helices of the coenzyme binding domain, and one of the two long α-helices that in GluDH connects the two domains. This prediction is supported in the case of LeuDH (Baker et al., 1995), and parts of this core structure are conserved also in DapDH. Thus the five β-strands (B1−B5) and four α-helices (A1−A3 and A10) of the dinucleotide binding domain are conserved, in spite of the fact that A10 is distant in primary sequence from the rest of the nucleotide binding fold. The α-helix connecting the dinucleotide binding domain to the substrate binding domain (A5 in DapDH) is rotated about 100° with respect to the position it occupies in either GluDH or LeuDH. The central six-stranded β-sheet of the substrate binding domain is conserved in all three structures, although the direction of some of the strands is reversed and their length varies, but none of the α-helices in this domain appear to be structurally conserved. Analysis of the residues that interact with the glutamate in GluDH (Stillman et al., 1993) and those proposed to interact with DAP in DapDH shows that they all belong either to the conserved β-sheet or to the conserved helices (A5 and A10 in DapDH). Thus, if we consider DapDH as a member of the same amino acid dehydrogenase family, the conserved core needs to be redefined without the inclusion of the three substrate binding domain helices. Another substantial dif-

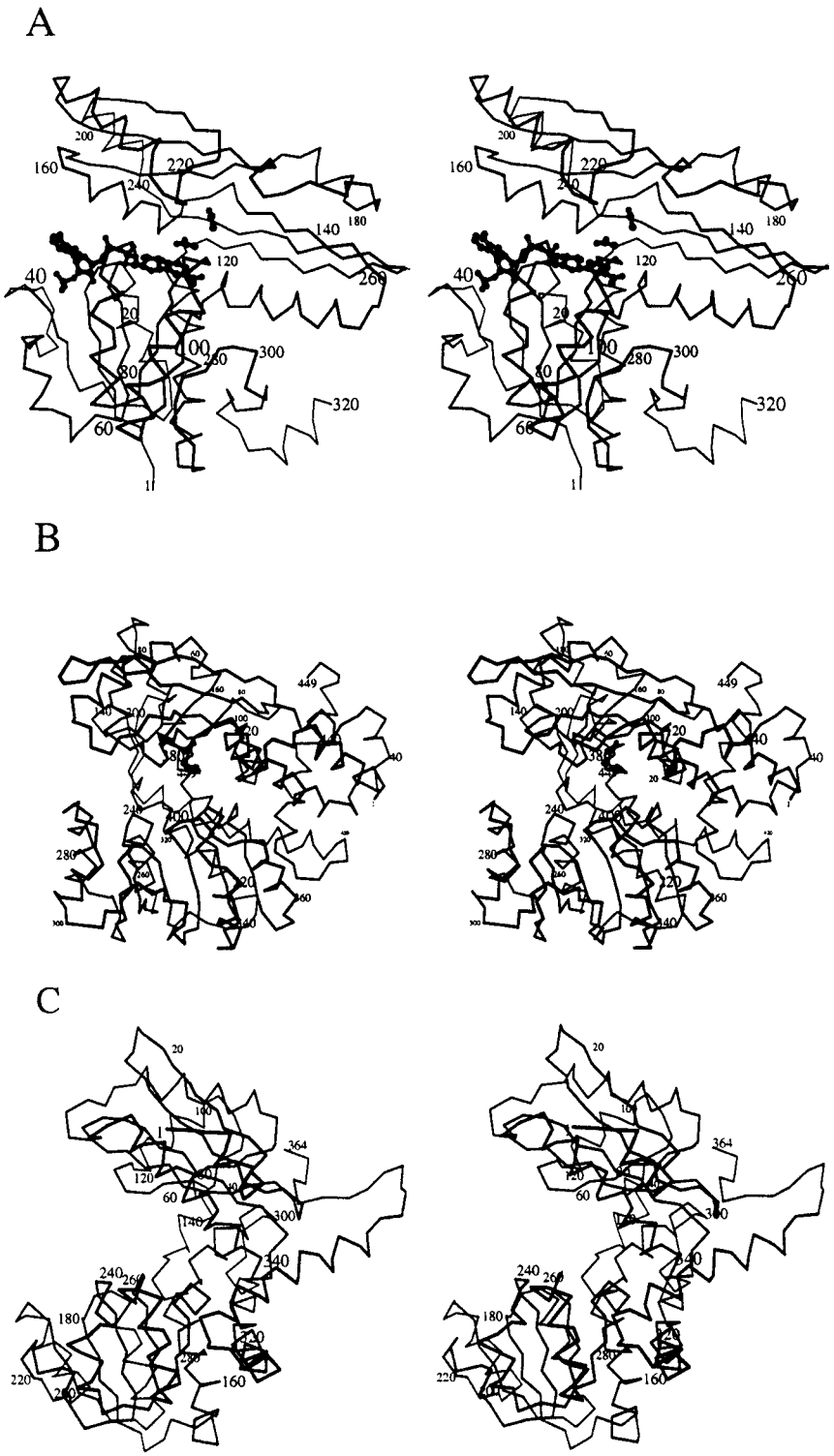

FIGURE 8: Stereoviews of the Cα traces for (A) DapDH, (B) GluDH, and (C) LeuDH. Numbers indicate every 20th residue. This figure was generated with MOLSCRIPT (Kraulis, 1991).

ference is the relative orientation of the two half-sheets in which the six-stranded β-sheet can be divided (B6, B10, B11, lower portion of the sheet, and B7, B8, B9, upper portion, in DapDH and the corresponding Bc, Be, Bf and Ba, Bb, Bd in GluDH; Baker et al., 1992b). While the upper portions are structurally comparable (B6, B10, and B11 and Bc, Bd, and Bf), the two lower portions appear to be rotated about 90° with respect one to another, and these strands are much longer in DapDH. This different orientation affects both the binding site and the mode of dimer formation. In GluDH, residues involved in the binding of the substrate mainly belong to β-strands c, e, and f, while β-strands a, b, and d contribute to the dimer formation. In DapDH, active site residues are mainly from β-strands 7, 8, and 9, and dimer formation involves β-strands 6, 10, and 11. The result is that while the dimers are generated by interactions between residues of the substrate binding domain, their shape is different. In GluDH and LeuDH, the two dinucleotide binding domains are at the opposite ends of the central β-sheet; in DapDH they are side by side. The DapDH dimer is much more compact than either GluDH or LeuDH, and this may be the reason why DapDH is a dimer in solution

that does not further oligomerize into hexamers or octamers. Lastly, in both GluDH and LeuDH the substrate binding domain is at the N-terminus, and the dinucleotide binding domain is at the C-terminus of the polypeptide. In DapDH, these are reversed, with the dinucleotide binding domain located at the N-terminus and the substrate binding domain in the C-terminus. There does not appear to be any structural or functional preference for one or the other domain assignment.

Upon comparison of the GluDH and DapDH amino acid binding sites, the most striking observation is that the positions of the two substrates relative to the dinucleotide binding site are nearly identical. Both GluDH and LeuDH are type B enzymes that catalyze transfer of the *pro-S* hydrogen of reduced nucleotides (Baker et al., 1992b, 1995), while the present study requires that DapDH be a type A enzyme that catalyzes the transfer of the *pro-R* hydrogen. We suggest that L- and D-amino acid dehydrogenases react with opposite enantiomers by reversing the stereochemistry of hydride transfer between amino acid and nucleotide substrates rather than reversing the position of the substrate binding site with respect to the nicotinamide ring, as is the case for L- and D-hydroxy acid dehydrogenases (Goldberg et al., 1994). This opposite stereochemistry of hydride transfer is the result of using two different conformations for the nicotinamide ring. In both GluDH and LeuDH the nicotinamide ring is *syn*, and the transfer is from the *pro-S* hydrogen. In contrast, in DapDH the nicotinamide is *anti*, and thus without inverting the substrate position, the *pro-R* hydrogen is positioned for transfer to the substrate. This opposite orientation of the nicotinamide ring and carboxamide chain in type B and type A amino acid dehydrogenases may be related to the different position of A5 in GluDH and LeuDH versus DapDH. In all three enzyme−nucleotide complexes, residues in this helix are involved in interactions with the nicotinamide ring, and this helix occupies different positions in GluDH and LeuDH versus DapDH.

Structural Similarity to other Proteins. A search through the Brookhaven Data Bank of the three-dimensional protein structure using the DALI server (Holm & Sander, 1993) and the three-dimensional structure of DapDH as probe showed that the highest structural similarity existed between DapDH and the *E. coli* dihydrodipicolinate reductase (DHPR, 1dih), the enzyme immediately preceding DapDH in the diaminopimelate/lysine biosynthetic pathway. The two enzymes share only 17% sequence identity over the equivalent positions. Figure 9 shows an overlay of the Cα traces of DapDH and DHPR, as calculated by DALI. The side chains of residues that comprise the substrate binding regions in both molecules are highlighted. The program matched 202 residues (out of 320 DapDH residues and 273 DHPR residues), inclusive of the two dinucleotide binding domains, α-helix A5, and the β-strand system in the C-terminal domain. Both enzymes exist as two-domain proteins; the bound dinucleotide and the substrate binding region occupy similar areas in both enzymes, even if there is little or no similarity among the residues that form these regions. The reactions carried out by the two enzymes are quite similar, and they both require the appropriate positioning of the reducible substrate with respect to the bound nucleotide in a way suitable for hydride transfer from the *pro-R* position of the cofactor (this work; Reddy et al., 1995). The structural and stereochemical similarities between the two enzymes suggest that they could be evolutionally related, possibly derived from a precursor enzyme that had both functionalities (reductase and dehydrogenase) on the same polypeptide chain.

FIGURE 9: Overlay of the Cα traces of DapDH (yellow) and DHPR (light blue). The bound nucleotides and the residues that form the substrate binding site in both molecules are shown (orange for DapDH and blue for DHPR).

REFERENCES

Abbot, S. D., Lane-Bell, P., Sidhu, K. P. S., & Vederas, J. C. (1994) *J. Am. Chem. Soc. 116*, 6513−6520.

Alschul, S. T., Gish, W., Miller, W., Meyers, E. W., & Lipman, D. (1990) *J. Mol. Biol. 215*, 403−410.

Baker, P. J., Britton, K. L., Rice, D. W., Rob, A., & Stillmann, T. J. (1992a) *J. Mol. Biol. 228*, 662−671.

Baker, P. J., Britton, K. L., Engel, P. C., Farrants, G. W., Lilley, K. S., Rice, D. W., & Stillman, T. J. (1992b) *Proteins 12*, 75−86.

Baker, P. J., Turnbull, A. P., Sedelnikova, S. E., Stillman, T. J., & Rice, D. W. (1995) *Structure 3*, 693−705.

Berges, D. A., DeWolf, W. E., Dunn, G. L., Newman, S. J., Schmidt, J., Taggart, J., & Gilvarg, G. (1986) *J. Biol. Chem. 261*, 6160−6167.

Birktoft, J. J., & Banaszak, L. J. (1984) *Pept. Protein Rev. 4*, 1−46.

Brandën, C.-I., & Tooze (1991) *Introduction to Protein Structure*, pp 141−159, Garland, New York, NY.

Britton, K. L., Baker, P. J., Engel, P. C., Rice, D. W., & Stillman, T. J. (1993) *J. Mol. Biol. 234*, 938−945.

Brünger, A. T. (1992) *X-PLOR version 3 manual: a system for crystallography and NMR*, Yale University, New Haven, CT..

Brünger, A. T., Kuriyan, J., & Karplus, M. (1987) *Science 235*, 458−460.

Brunhuber, N. M. W., & Blanchard, J. S. (1994) *Crit. Rev. Biochem. Mol. Biol. 29*, 415−467.

Burnett, R. M., Darling, G. D., Kendall, D. S., Lequesne, M. E., Meyhew, S. G., Smith, W. W., & Ludwig, M. L. (1974) *J. Biol. Chem. 249*, 4383−4392.

Bystroff, C., Oatley, S. J., & Kraut, J. (1990) *Biochemistry 29*, 3263−3277.

Cowtan, K. D. (1994) *Jt. CCP4 and IESF-EACMB Newsl. Protein Crystallogr. 31*, 34−38.

Cowtan, K. D., & Main, P. (1996) *Acta Crystallogr. D52*, 43−48.

Davies, J. F., Delcamp, T. J., Prendergast, N. J., Ashford, V. A., Freisheim, J. H., & Kraut, J. (1990) *Biochemistry 29*, 9467−9479.
Eads, J. C., Scapin, G., Xu, Y., Grubmeyer, C., & Sacchettini, J. C. (1995) *Cell 78*, 325−334.
Evans, S. V. (1993) *J. Mol. Graphics 11*, 134−138.
Furey, W., & Swaminathan, S. (1986) *Am. Crystallogr. Assoc. Am. Meet. Program Abstr. 18*, 73.
Goldberg, J. D., Yoshida, T., & Brick, P. (1994) *J. Mol. Biol. 236*, 1123−1140.
Grant, G. A. (1989) *Biochem. Biophys. Res. Commun. 165*, 1371−1374.
Hol, W. G. J., van Dujien, P. T., & Berendsen, H. J. C. (1978) *Nature 273*, 443−446.
Holm, L., & Sander, C. (1993) *J. Mol. Biol. 233*, 123−138.
Howard, A. J. (1986) *A guide to data reduction for the Nicolet Imaging Proportional Counter: the XENGEN system*, Protein Engineering Department, GENEX Corp., 16020 Industrial Dr., Gaithersbury, MD 20877.
Ishino, S., Mizukami, T., Yamaguchi, K., Katsumata, R., & Araki, K. (1987) *Nucleic Acids Res. 15*, 3917.
Jones, T. A., Zou, J. Y., Cowan, S. W., & Kjeldgaard, M. (1991) *Acta Crystallogr. A43*, 489−501.
Karplus, P. A., & Schulz, G. E. (1989) *J. Mol. Biol. 210*, 163−180.
Karplus, P. A., Daniels, M. J., & Herriot, J. R. (1991) *Science 251*, 60−66.
Kindler, S. H., & Gilvarg, C. (1960) *J. Biol. Chem. 235*, 3532−3535.
Kraulis, P. J. (1991) *J. Appl. Crystallogr. 24*, 946−950.
Lam, L. K. P., Arnold, L. D., Kalantart, T. H., Kelland, J. G., Lane-Bell, P. M., Palcic, M. M., Pickard, M. A., & Vederas, J. C. (1988) *J. Biol. Chem. 263*, 11814−11819.
Laskowski, R. A., MacArthur, M. W., Moss, S. D., & Thornton, J. M. (1993) *J. Appl. Crystallogr. 26*, 283−291.
Misono, H., & Soda, K. (1980) *J. Biol. Chem. 255*, 10599−10605.
Misono, H., Nagasaki, S., & Soda, K. (1981) *Agric. Biol. Chem. 45*, 1455−1460.
Misono, H., Ogasawara, M., & Nagasaki, S. (1986a) *Agric. Biol. Chem. 50*, 1329−1330.
Misono, H., Ogasawara, M., & Nagasaki, S. (1986b) *Agric. Biol. Chem. 50*, 2729−2734.
Nicholls, A., Sharp, K., & Honig, B. (1991) *Proteins: Struct., Funct., Genet. 11*, 281.
Rao, S. T., & Rossmann, M. G. (1973) *J. Mol. Biol. 76*, 241.
Read, R. J. (1986) *Acta Crystallogr. A42*, 140−149.
Reddy, S. G., Sacchettini, J. C., & Blanchard, J. S. (1995) *Biochemistry 34*, 3492−3501.
Reddy, S. G., Scapin, G., & Blanchard, J. S. (1996). *Proteins: Struct., Funct., Genet. 25*, 514−516.
Richardson, J. S. (1981) *Adv. Protein Chem. 34*, 167−339.
Roberts, A. L. U., & Brünger (1995) *Acta Crystallogr. D51*, 990−1002.
Rossmann, M. G., Liljas, A., Brandën, C.-I., & Banaszak, L. J. (1975) *Enzymes (3rd Ed.) 11A*, 61−102.
Scapin, G., Grubmeyer, C., & Sacchettini, J. C. (1994) *Biochemistry 33*, 1287−1294.
Scapin, G., Blanchard, J. S., & Sacchettini, J. C. (1995) *Biochemistry 34*, 3502−3512.
Schrumpf, B., Schwarzer, A., Kalinowiski, J., Pühler, A., Eggeling, L., & Sahm, H. (1991) *J. Bacteriol. 173*, 4510−4516.
Smith, J. L., Zelulec, J., Warey, J. J.-P., Niu, L., Switzer, R. L., Zalkin, H., & Setow, Y. (1994) *Science 264*, 1427−1433.
Stillman, T. J., Baker, P. J., Britton, K. L., & Rice, D. W. (1993) *J. Mol. Biol. 234*, 1131−1139.
Sundharadas, G., & Gilvarg, G. (1967) *J. Biol. Chem. 242*, 3983−3988.
Tronrud, D. E., Ten Eyck, L. F., & Mathews, B. W. (1988) *Acta Crystallogr.. A43*, 489−501.
Wang, B.-C. (1985) *Methods Enzymol. 115*, 90−112.
Watenpaugh, K. D., Sieker, L. C., & Jensen, L. H. (1973) *Proc. Natl. Acad. Sci. U.S.A. 70*, 3857−3860.
White, P. J. (1983) *J. Gen. Microbiol. 129*, 739−749.
Wierenga, R. K., De Maeyer, M. C. H., & Hol, W. G. J. (1985) *Biochemistry 24*, 1346−1357.
Wierenga, R. K., Terpstra, P., & Hol, W. G. J. (1986) *J. Mol. Biol. 187*, 101−107.
Yip, K. S. P., Stillman, T. J., Britton, K. L., Artymiuk, P. J., Baker, P. J., Sedelnikova, S. E., Engel, P. C., Pasquo, A., Chiaraluce, R., Consalvi, V., Scandurra, R., & Rice, D. W. (1995) *Structure 3*, 1147−1158.

BI961628I